ADVANCING EARTH AND SPACE SCIENCE

Earth's Future

RESEARCH ARTICLE
10.1029/2022EF002880

Key Points:

- Calculations using radar-based global elevation models available to date have generally underestimated the extent of lowest coastal areas that are most exposed to sea-level rise (SLR)
- A recent lowland elevation model (global LiDAR lowland DTM (GLL_DTM_v2)) derived from only satellite LiDAR data is currently most accurate, we recommend such LiDAR data to be used in SLR impact assessments
- Applying this model we find that the greatest increase in global coastal area below mean sea level will occur in the early stages of SLR, contrary to earlier assessments

Supporting Information:

Supporting Information may be found in the online version of this article.

Correspondence to:

R. Vernimmen,
ronald.vernimmen@dataforsustainability.com

Citation:

Vernimmen, R., & Hooijer, A. (2023). New LiDAR-based elevation model shows greatest increase in global coastal exposure to flooding to be caused by early-stage sea-level rise. *Earth's Future*, *11*, e2022EF002880. https://doi.org/10.1029/2022EF002880

Received 10 MAY 2022
Accepted 30 NOV 2022
Corrected 20 JAN 2023

This article was corrected on 20 JAN 2023. See the end of the full text for details.

New LiDAR-Based Elevation Model Shows Greatest Increase in Global Coastal Exposure to Flooding to Be Caused by Early-Stage Sea-Level Rise

Ronald Vernimmen[1] and Aljosja Hooijer[2,3]

[1]Data for Sustainability, Axel, The Netherlands, [2]Deltares, Inland Water Systems Unit, Delft, The Netherlands, [3]NUS Environmental Research Institute (NERI), National University of Singapore, Singapore, Singapore

Abstract The latest projections indicate that sea-level rise (SLR) is certain to exceed 2 m in coming centuries, and a rise by 4 m is considered possible. Radar-based land elevation models applied to date suggest that the increase of area below mean sea level, that is potentially exposed to permanent flooding, will accelerate as SLR proceeds, being relatively limited initially. However, applying new and more accurate satellite LiDAR elevation data we find the opposite pattern, with the fastest increase in the area of exposed land occurring in the early stages of SLR. In one-third of countries most of this increase will be caused by the first meter of SLR and in nearly all within the first 2 m. We conclude that in many regions the time available to prepare for increased exposure to flooding may be considerably less than assumed to date, and that better elevation data will support timely preparations. The global LiDAR lowland DTM (GLL_DTM_v2) elevation data set developed for this assessment is available in the public domain.

Plain Language Summary The latest sea-level rise (SLR) projections indicate that future sea levels are certain to exceed 2 m and a rise by 4 m is considered possible. Land elevation models applied to date suggest that the increase of land area below sea level will be limited at first but will go faster when SLR continues. When we apply a new and more accurate elevation model we find the opposite pattern, with the fastest increase during the early stages of SLR. In one-third of countries most of this increase will be during the first meter of SLR, and in almost all within the first 2 m. We conclude that in many regions the time available to prepare for increased exposure to flooding may be considerably less than assumed to date, and that better elevation data will support timely preparations. The global LiDAR lowland DTM (GLL_DTM_v2) elevation data set developed for this assessment is available in the public domain.

1. Introduction

The latest (6th) Assessment Report of the International panel for Climate Change (IPCC, 2021) provides sea-level rise (SLR) projections not only for 2100 but also for the centuries beyond. While SLR in the low carbon emission scenario (SSP1-2.6) is unlikely to exceed 0.62 m by 2100, this could increase to over 3 m by 2300. In the high emission scenario (SSP5-8.5) SLR could approach 2 m by 2150 (0.98–1.88 m) and 7 m by 2300. In addition, rates of land subsidence caused by drainage and groundwater abstraction are of the same order as SLR in many coastal regions and in some urban areas even much higher (Herrera-García et al., 2021; Hooijer & Vernimmen, 2021; Nicholls et al., 2021; Syvitski et al., 2009). It therefore is likely that relative SLR (hereafter: SLR), which includes land subsidence, will in most densely populated coastal areas reach 1 m well before 2150, and 4 m in centuries to come.

For climate change adaptation, the relevance of SLR lies mostly in increased coastal exposure to flooding, which may translate either in actual flooding or in increased cost of adaptation measures. The timing of mean sea level (MSL) exceeding land elevation as SLR proceeds may be the most meaningful parameter to exposure projections especially in parts of the world with limited coastal protection, as this implies the possibility of permanently losing land to the sea. Determining this timing requires application of a global digital elevation model (GDEM). However, existing GDEMs have been found to be too inaccurate for SLR related assessments, amongst others because they are created using radar data that is unable to penetrate dense vegetation and also measures elevations of non-ground features in built-up areas (Gesch, 2018; Hooijer & Vernimmen, 2021).

With the recent (2018) launch of Earth observation satellites carrying LiDAR sensors that are known to have much higher vertical accuracy than earlier radar data sources, a new generation of global elevation models is evolving.

10.1029/2022EF002880

The first version of such a model (Global LiDAR Lowland DTM; GLL_DTM_v1) at 0.05-degree (∼5 km near the equator) horizontal resolution was published in 2020 (Vernimmen et al., 2020) and applied to estimate global coastal land area distribution below 2 m + MSL (Hooijer & Vernimmen, 2021). The ICESat-2 LiDAR data is used because it is the most accurate of the new satellite LiDAR datasets at present (Liu et al., 2021). As these data continued to come in, a higher horizontal resolution elevation model (GLL_DTM_v2) at 0.01-degree (∼1 km near the equator) is developed and presented here that is suitable for refined analyses.

The radar-based SRTM was the first GDEM and is still most commonly used in global coastal SLR impact assessments to date (e.g., Brown et al., 2021; Jevrejeva et al., 2018; Nicholls et al., 2021; Schuerch et al., 2018; Syvitski et al., 2009) despite having low vertical accuracy by any measure (Vernimmen et al., 2020). The MERIT GDEM is also often used in global and regional assessments (Haasnoot et al., 2021; Kirezci et al., 2020) but while having somewhat improved accuracies compared to its source SRTM it still cannot be used with high confidence in SLR assessments (Gesch, 2018; Hooijer & Vernimmen, 2021). A more recent development is the use of ICESat-2 LiDAR data to improve vertical accuracy of NASADEM (CoastalDEM v2.1; Kulp & Strauss, 2021) and Copernicus DEM (FABDEM; Hawker et al., 2022).

As existing GDEMs all generally overestimate surface elevation, especially in forested and built-up areas (Gesch, 2018; Hawker et al., 2022), they have in common that the rate of increase of land below MSL would in most regions be expected to accelerate as SLR progresses, with the increase in flood exposure being underestimated initially. We have applied the new GLL_DTM_v2 to investigate whether this relatively limited initial impact followed by an acceleration is a valid expectation or an artefact of GDEM inaccuracy.

Our assessment considers only the position of the land surface relative to MSL, that is, we quantify potential exposure to flooding rather than vulnerability. Whether and how the land will increasingly flood due to SLR depends on factors such as the presence and effectiveness of flood defenses as well as trends in extreme storm surges, rainfall and extreme river levels.

The manuscript is organized as follows. We first present the GLL_DTM_v2 GDEM with an accuracy assessment including a comparative validation of other GDEMs commonly applied in flood risk assessments. We then apply GLL_DTM_v2 to analyze the global distribution and timeline patterns of land exposure to SLR between 1 and 4 m and compare the results with those using the other GDEMs.

2. Materials and Methods

2.1. Generating GLL_DTM_v2

Land elevation is determined from the second version of the GLL_DTM_v2 at 0.01-degree horizontal resolution (i.e., ∼1 km near the equator). This version is a refinement of the GLL_DTM_v1 described by Vernimmen et al. (2020) at 0.05-degree horizontal resolution. We now apply more data filtering steps to remove outliers in the ICESat-2 data that can have a greater impact at this higher resolution as fewer data segments are available in each grid cell. The land mask is improved to include the mangrove distribution data set of Global Mangrove Watch (Bunting et al., 2018) for the year 2016 and excludes cells which consist of water for more than 50% according to the ASTER water body data set (Abrams et al., 2020).

The model is created from version 5 of the ICESat-2 ATL08 geophysical data product provided by the National Snow and Ice Data Center (Neuenschwander et al., 2021). The data collection period of 14 October 2018–8 June 2022 used here exceeds the planned 3-year operational lifespan of ICESat-2 (Neuenschwander & Pitts, 2019) and ensures near-optimal data coverage from this source. We resampled the terrain height ("h_te_median" variable) from 58.6 million 100 m data segments along all 203,351 currently available ICESat-2 near-polar ground tracks to a 0.01-degree land grid by calculating the median elevation of 100 m data segments within each 0.01-degree grid cell. Before resampling, all data segments with a median terrain height below −7 m + MSL are removed because they are considered unrealistic in coastal lowland, noting that −7 m + MSL is the lowest land elevation value found in pumped polders in the Netherlands. To limit the effect of remaining outliers on median elevation values only grid cells with 5 or more 100 m data segments are retained. Of all GLL_DTM_v2 grid cells, 21.6% are without data segments and 6.8% have 1 to 4 data segments. From the 71.6% of grid cells with data segments (on average 24 segments per grid cell), outliers are identified and removed if the respective cell has at least four neighbors with data, is not bordered by water cells and the elevation deviates more than 2 m from the median elevation of the immediate 8 (both in cardinal and ordinal directions) neighbor grid cells (2.4% of data cells, 1.7% of all grid cells). If the respective cell has less than 4 neighbors and is not bordered by water cells, elevation values below 0 m + MSL are also considered outliers and are removed (0.2% of data cells, 0.1% of all grid cells). Values for the resulting set of "no data" grid cells (30.3% of the cell total after outlier removal) are interpolated between data cell values through inverse distance weighted (IDW) interpolation. The implemented IDW method only takes into account the nearest raster cells that have a value in all directions up to a distance of 10 km (99.9% of grid cell center points with data are within 10 km of at least one neighbor, 85.2%, 98.8%, and 99.6% of grid cell center points are within 1, 3 and 5 km, respectively). We apply a power of 2 to determine the weight from distance.

The ICESat-2 data are referenced to the WGS84 ellipsoid. The ICESat-2 data are transformed to the EGM96 geoid using the 5-min version available from https://sourceforge.net/projects/geographiclib/files/geoids-distrib/. To convert the vertical datum from the EGM96 geoid to MSL, we use the mean dynamic ocean topography (MDT), which is the difference between the mean sea surface and the geoid. Following Muis et al. (2017), we use an estimate by Rio et al. (2014), who calculated the MDT by combining geodetic data (i.e., altimetric mean sea surface over the period 1993–2012 and an accurate geoid) with in situ data, at 0.25-degree resolution (http://www.aviso.altimetry.fr/). For referencing to MDT on land, the closest value at sea is used.

2.2. Global Digital Elevation Models (GDEMs)

Nine near-global DEMs that are available in the public domain with some of them previously being applied in global and local assessments of flood risk (Brown et al., 2018, 2021; Haasnoot et al., 2021; Jevrejeva et al., 2018; Kirezci et al., 2020; Koks et al., 2019; Neumann et al., 2015; Nicholls et al., 2021; Schuerch et al., 2018; Zhang et al., 2019), are compared with the GLL_DTM_v2. These are SRTM v4.1 (Jarvis et al., 2008), MERIT-DEM (Yamazaki et al., 2017), CoastalDEM v2.1 (Kulp & Strauss, 2021), TanDEM-X (Rizzoli et al., 2017), Copernicus DEM GLO-30 v2020-02 (Airbus, 2020), FABDEM (Hawker et al., 2022), NASADEM v1 (Crippen et al., 2016), ASTER GDEM v3 (Abrams et al., 2020), and ALOS AW3D30 v3.2 (Tadono et al., 2016). The first seven are radar-based or apply a machine-learning combination of radar and ICESat-2 LiDAR data (CoastalDEM v2.1, FABDEM), while the latter two are optical-based. The first four have a horizontal resolution of 3-arc- seconds (~90 m at the equator) while the latter five have a horizontal resolution of 1-arc-second (~30 m at the equator). They cover areas varying from 60°N to 56°S (SRTM, NASADEM and CoastalDEM v2.1), 90°N–60°S (MERIT), 80°N–60°S (FABDEM), 82°N–82°S (AW3D30), 83°N–83°S (ASTER), 84°N–84°S (TanDEM-X) to 84°N–90°S (Copernicus DEM).

All GDEM elevations except TanDEM-X, Copernicus DEM and FABDEM are orthometric heights referenced to the EGM96 geoid. TanDEM-X is referenced to the WGS84 ellipsoid and transformed to the EGM96 geoid. Both Copernicus DEM and FABDEM are referenced to the WGS84 ellipsoid and have orthometric heights referenced to the EGM2008 geoid. All GDEMs are converted from the EGM96 geoid to MSL using the MDT (Rio et al., 2014) and from EGM2008 geoid to MSL using the CNES-CLS18 MDT (Mulet et al., 2021). After transformation, the GDEMs are resampled to the same 0.01-degree grid as GLL_DTM_v2, by calculating the median of elevation values at native resolution within each 0.01-degree grid cell.

2.3. GDEM Vertical Accuracy Assessment by Comparison With Local DTMs

The vertical accuracy of the GLL_DTM_v2 and other GDEMs is determined through validation against existing well-described and accurate local DTMs for major lowland regions across three continents are used: (a) The Everglades in the USA, (b) The Netherlands lowlands, and (c) the Mekong Delta in Vietnam; the first two of these are based on airborne LiDAR, whereas the Mekong Delta data set is generated from a topographic map based on field surveys. The latter DTM is reported to have a mean deviation of 0.2 m and mean absolute deviation of 0.6 m against local benchmarks (Minderhoud et al., 2019), whereas for the two LiDAR-derived DTMs vertical accuracies are not provided in scientific publications. However, the LiDAR data used in the creation of the DTMs are within 0.245 m (FEMA, 2022) and 0.15 m (AHN3, 2022) at 95% confidence levels for The Everglades and The Netherlands, respectively. The validation datasets are further described in Vernimmen et al. (2020).

In addition to validation at the GLL_DTM_v2 horizontal resolution of ~1 km, validation for the most accurate GDEMs (Table 1) is also carried out at native horizontal resolution of ~90 m (CoastalDEM v2.1) and ~30 m (FABDEM) for which GLL_DTM_v2 and the local DTMs are resampled to the same native horizontal resolution as the respective GDEMs. For comparison, GLL_DTM_v2 is downscaled to ~90 m (12 × 12 cells within original

10.1029/2022EF002880

Table 1
Vertical Accuracy of GLL_DTM_v2 and Existing GDEMs for Areas Below 10 m + MSL (as Compared to Local DTMs), at 0.01-Degree Horizontal Resolution

	ICESat-2 LiDAR-based	Radar-based (ICESat-2 LiDAR corrected)		Radar-based					Optical-based	
Statistical measure	GLL_DTM_v2	CoastalDEM 2.1	FABDEM	SRTM	MERIT	NASADEM	TanDEM-X	CopernicusDEM	ASTER	AW3D30
Everglades NOAA sea-level rise DEM (14,121 km^2)										
Within 0.5 m [%]	86.6	34.7	50.2	1.1	7.6	22.7	23.7	36.3	0.5	1.3
Within 1 m [%]	95.9	63.4	73.6	2.7	19.6	43.2	39.9	58.3	1.1	3.9
ME [m]	0.05	−0.03	0.66	4.44	2.05	0.83	1.80	1.34	7.98	4.12
MAE [m]	0.27	0.86	0.86	4.45	2.15	1.57	1.82	1.45	7.99	4.12
RMSE [m]	0.44	1.06	1.36	4.96	2.59	2.16	2.67	2.40	8.69	4.75
Netherlands AHN3 (19,047 km^2)										
Within 0.5 m [%]	78.8	48.6	77.6	19.0	17.2	44.7	71.9	63.3	2.3	27.6
Within 1 m [%]	92.2	80.5	95.8	43.5	45.8	73.2	81.8	88.1	4.6	52.5
ME [m]	−0.09	−0.38	−0.21	−0.69	0.96	0.39	0.52	0.10	8.44	−0.14
MAE [m]	0.37	0.66	0.39	1.27	1.20	0.91	0.67	0.67	8.51	1.22
RMSE [m]	0.65	0.93	0.61	1.63	1.46	1.52	1.56	1.37	9.42	1.76
Mekong Delta TOPODEM (38,510 km^2)										
Within 0.5 m [%]	74.5	49.8	68.2	32.2	12.8	33.3	47.9	66.3	0.1	30.2
Within 1 m [%]	96.2	78.9	86.9	61.2	33.5	61.3	74.1	81.2	0.2	56.1
ME [m]	0.16	0.03	0.23	−0.11	1.31	−0.33	0.88	0.36	6.55	0.21
MAE [m]	0.37	0.64	0.52	1.01	1.42	0.97	0.93	0.70	6.55	1.11
RMSE [m]	0.48	1.00	1.19	1.53	1.78	1.53	1.69	1.59	7.21	1.69
Mean of 3 areas (71,678 km^2)										
Within 0.5 m [%]	80.0	44.4	65.3	17.4	12.5	33.6	47.9	55.3	1.0	19.7
Within 1 m [%]	94.8	74.3	85.4	35.8	32.9	59.2	65.3	75.9	2.0	37.5
ME [m]	0.04	−0.13	0.23	1.21	1.44	0.30	1.07	0.60	7.65	1.40
MAE [m]	0.34	0.72	0.59	2.24	1.59	1.15	1.14	0.94	7.68	2.15
RMSE [m]	0.53	0.99	1.06	2.70	1.94	1.74	1.97	1.79	8.44	2.74

Note. Presented are mean elevation differences (ME = mean error, MAE = mean absolute errror) between the local DTM, GLL_DTM_v2, and existing GDEMs, as well as RMSE and the area percentage differences within ranges −1 to +1 m and −0.5 to +0.5 m. Based on this analysis, CoastalDEM 2.1 and FABDEM are the most accurate after GLL_DTM_v2, for coastal land below 10 m + MSL.

0.01-degree grid) and ~30 m (36 × 36 cells) resolution. The local DTMs are resampled by calculating the median of elevation values at native resolution within each ~90 and ~30 m grid cell.

We also determine vertical accuracy separately for built-up and forested areas at different horizontal resolutions. A grid cell is considered built-up if more than 50% is classified as built-up according to the World Settlement Footprint 2015 data set at 10 m horizontal resolution (Marconcini et al., 2020). A cell is considered forested if more than 50% is classified as having a canopy height of more than 3 m according to the Global Forest Canopy Height 2019 data set derived from GEDI satellite LiDAR data at 30 m horizontal resolution (Potapov et al., 2021). Since the extent of GEDI (51.6°N–51.6°S) does not fully cover The Netherlands, forest validation is only carried out over The Everglades and the Mekong delta.

2.4. Current Coastal Lowland Population Distribution

Global population distribution in 2020 is determined from the UN adjusted Gridded Population of the World database (Centre for International Earth Science Information Network (CIESIN) & Columbia University, 2018).

2.5. Calculation of Elevation Below 2 m + MSL Within Major Deltas of the World

Using SRTM, Syvitski et al. (2009) identified 33 deltas which have large areas below 2 m. Considering the low vertical accuracy of the SRTM data used in that study we calculated for the same deltas the areas below 2 m + MSL using GLL_DTM_v2, to demonstrate the effect of applying improved elevation data. The spatial extent of these deltas is obtained from https://www.globaldeltarisk.net/data.html referring to Tessler et al. (2015).

2.6. Coverage of Analysis and Area Calculations

All analyses are within the SRTM extent (60°N–56°S) to allow comparison amongst GDEMs. All areas presented are calculated applying the equal area projection (Brodzik et al., 2014). Area calculations under projected SLR level apply the "bathtub" approach (Gesch, 2018), that is, coastal water levels are projected inland across the floodplain, not considering flood defenses or other barriers.

3. Results and Discussion

3.1. Accuracy of GLL_DTM_v2 Compared to Other GDEMs

Validated at 0.01-degree (~1 km) horizontal resolution against local elevation models covering 71,678 km^2 (2.3% of global coastal land below 10 m + MSL) for The Everglades (USA), The Netherlands, and Mekong Delta (Vietnam), GLL_DTM_v2 has a Mean Absolute Error (MAE) and Root Mean Square Error (RMSE) of 0.34 and 0.53 m (Table 1, Figure S1 in Supporting Information S1), respectively, compared to 0.59–7.68 m/0.99–8.44 m for other published GDEMs (Table 1). Furthermore, we find that GLL_DTM_v2 is accurate within 0.5 and 1 m over 80.0/94.8% which is higher than the 44.4/74.3% and 65.3/85.4% achieved by CoastalDEM v2.1 and FABDEM over the combined validation areas (Table 1).

On average, MAE improves from 0.33 to 0.32 m and RMSE from 0.54 to 0.50 m after outlier removal (Table S1 in Supporting Information S1). Interpolation of "no data" grid cells has limited impact on overall accuracy (MAE from 0.32 to 0.34 m and RMSE from 0.50 to 0.53 m; Table S1, Figure S2 in Supporting Information S1), supporting the use of the applied IDW interpolation method in lowland areas that tend to be flat.

3.2. Accuracy of Other GDEMs, and Implications to SLR Impact Assessments

The most commonly applied GDEM, SRTM, has an MAE of 2.24 m and RMSE of 2.70 m when resampled to 0.01-degree resolution for coastal land below 10 m + MSL (Table 1). Despite major improvements compared to SRTM and other earlier products, considerable inaccuracies remain in CoastalDEM v2.1 and FABDEM with MAE/RMSE of 0.72/0.99 m and 0.59/1.06 m at the 0.01-degree resolution and 0.86/1.18 m and 0.75/1.29 m at native resolution of ~30–90 m (Table S2 in Supporting Information S1). It should be noted that vertical GDEM accuracy needs to be at least half the SLR increment to assess exposed land areas at the 68% confidence level

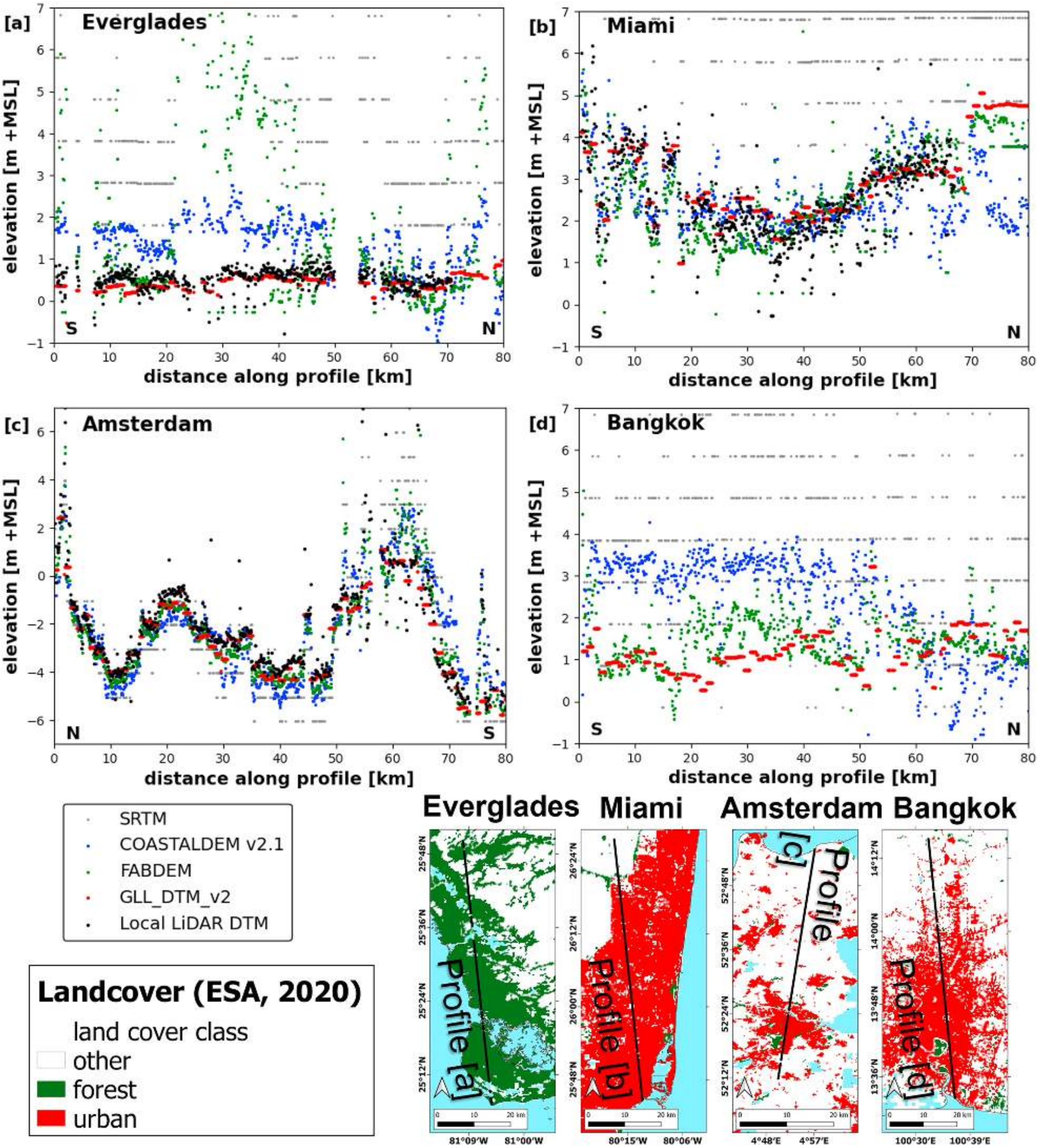

Figure 1. (a, c) Elevation cross sections along ICESat-2 flight lines covering (a) mangrove forest and coast in the Everglades (USA) (b) Miami (USA), (c) Amsterdam (Netherlands) and (d) Bangkok (Thailand). Location of the cross sections is shown with in the background European Space Agency Climate Change Initiative Land Cover for 2020, reclassified to forest and urban cover (ESA, 2020). Shown are GLL_DTM_v2 and selected GDEMs at native resolution (SRTM and CoastalDEM v2.1 at ~90 m and FABDEM at ~30 m) as well as local airborne LiDAR data for Everglades and Miami (NOAA Sea Level Rise DEM, 2020) and Amsterdam (AHN3, 2019). Note that NOAA LiDAR data are not available beyond ~70 km along the profile.

(Gesch, 2018). With RMSEs above 1 m, these GDEMs therefore allow confident quantification of exposed area for SLR exceeding 2 m whereas GLL_DTM_v2 allows this for SLR around 1 m.

3.3. Effect of Horizontal Resolution and Land Cover on Vertical Accuracy

While the 0.01-degree (∼1 km) horizontal resolution of GLL_DTM_v2 is lower than the horizontal resolution of other GDEMs we demonstrate that the impact of horizontal resolution on vertical accuracy is limited in coastal lowlands, as these tend to be flat. At resampled horizontal resolutions of ∼1 km, ∼90, and ∼30 m, we find MAE values for GLL_DTM_v2 of 0.34/0.43/0.45 m, and RMSE of 0.53/0.68/0.71 m, respectively (Table S2, Figure S3 in Supporting Information S1), which indicates higher accuracy than the other GDEMs at any resolution (Table S2 in Supporting Information S1). This is especially true for forested areas and dense urban areas where GLL_DTM_v2 outperforms all GDEMs by at least a factor 2 (Table S3, Figure S4 in Supporting Information S1). This is also illustrated in Figure 1 where elevation profiles over four areas demonstrate that GLL_DTM_v2 closely resembles the topography as derived from local airborne LiDAR DTMs where available, while CoastalDEM v2.1 has major outliers both upwards and downwards especially over urban areas, and major vegetation signals remain visible over forest (Everglades) in both CoastalDEM v2.1 and FABDEM. Moreover, vertical accuracy of GLL_DTM_v2 is relatively consistent across land cover types with MAE values of 0.34, 0.30, and 0.56 m, and RMSE of 0.53 m, 0.46 and 0.80 m for all land, forested and built-up areas, respectively (Tables S2–S4 in Supporting Information S1). This consistency amongst land cover types is lower for the other GDEMs, with a range in MAE from 0.13 to 0.98 m and RMSE from 0.53 to 1.83 m for CoastalDEM v2.1 and FABDEM, respectively (Tables S2–S4 in Supporting Information S1).

3.4. Estimates of Exposed Area Applying GLL_DTM_v2 and Other GDEMs

Application of GLL_DTM_v2 results (within SRTM extent) in global areas below MSL of 123 thousand km^2 by 2020 (SLR = 0 m) and 482/937/1,586 thousand km^2 after 1, 2, and 4 m SLR, respectively (Figures 2 and 3, Table S5 in Supporting Information S1), compared to 7–179, 7–376, 9–790, and 42–1,554 thousand km^2 for existing published GDEMs for these same amounts of SLR (Figure 2, Tables S6–S10 in Supporting Information S1). Within the full global extent, pole to pole, the area below 4 m + MSL is 1,749 thousand km^2, indicating that 9.3% of global coastal lowland is not covered by SRTM-based GDEMs.

The increase in coastal land area below MSL according to GLL_DTM_v2 (within SRTM extent) is 359 thousand km^2 over the first meter of SLR (from 123 to 482 thousand km^2) and 455 thousand km^2 over the second meter of SLR (from 482 to 937 thousand km^2). Combined, the total area below MSL after 2 m of SLR is 1.2–2.4 times higher when compared to seven GDEMs that are fully or partly radar-based (Figure 2, Table S5–S9 in Supporting Information S1). After 2 m of SLR the increase in coastal land area below MSL gradually decreases until a total area of 1,586 thousand km^2 at 4 m of SLR, 1.9 times higher when compared to SRTM. Acceleration of land area below MSL as SLR progresses is found using SRTM, MERIT, NASADEM and the optical-based GDEMs,

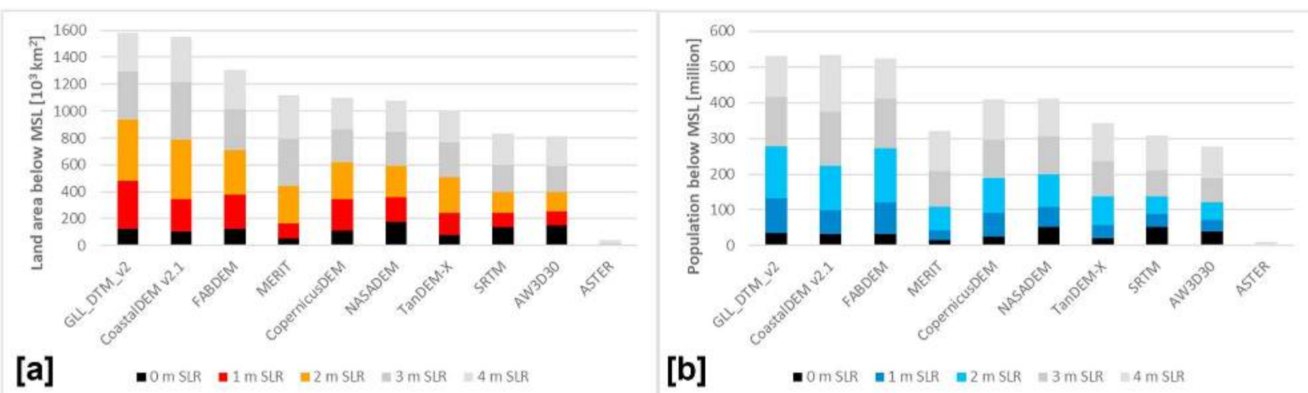

Figure 2. (a) Land area and (b) population below MSL after 0 (2020), 1, 2, 3, and 4 m of sea-level rise (SLR) for GLL_DTM_v2 as compared with GDEMs (all within SRTM extent). Population data from (Centre for International Earth Science Information Network (CIESIN) & Columbia University, 2018). In Tables S5–S10 in Supporting Information S1 details for 26 countries with over 2.0 million people currently (2020) living on land below 4 m + MSL. Sources are ranked by total land below MSL at 4 m SLR.

whereas the other four radar-based GDEMs also show a gradual deceleration in land area below MSL after 2 m of SLR but not to the same degree as GLL_DTM_v2. This demonstrates that the least accurate GDEMs yield the least realistic assessments of coastal land exposed to SLR.

Of the 26 countries with the greatest populations on land below 4 m + MSL (Table S2 in Supporting Information S1), GLL_DTM_v2 demonstrates that 5 (19%) and 24 (92%) will have over 50% of such land below MSL after 1 and 2 m SLR respectively, whereas application of SRTM would yield 4 (15%) and 12 (46%) countries (Figure 3). For some individual countries the differences are even more striking. Nigeria for example, will see a 16,242 km^2 increase of land below MSL over the first meter of SLR and 2,198 km^2 over the fourth according to GLL_DTM_v2 (Figure 4, Table S5 in Supporting Information S1), whereas SRTM suggests this would be 58 and 1,998 km^2 respectively, that is, a sharp acceleration from a far lower base (Figure 4, Table S6 in Supporting Information S1). Similar major differences are seen for Bangladesh, Brazil, Cameroon, Indonesia, Malaysia, Mozambique, Philippines, Sri Lanka and Thailand, with SRTM and most derived GDEMs yielding areas below MSL that are unrealistically low overall, but especially in the first meter of SLR (Tables S6–S10 in Supporting Information S1). The recent GDEMs that used ICESat-2 LiDAR data to correct NASADEM (CoastalDEM v2.1) and Copernicus DEM (FABDEM) yield similar patterns as GLL_DTM_v2 for many countries, but

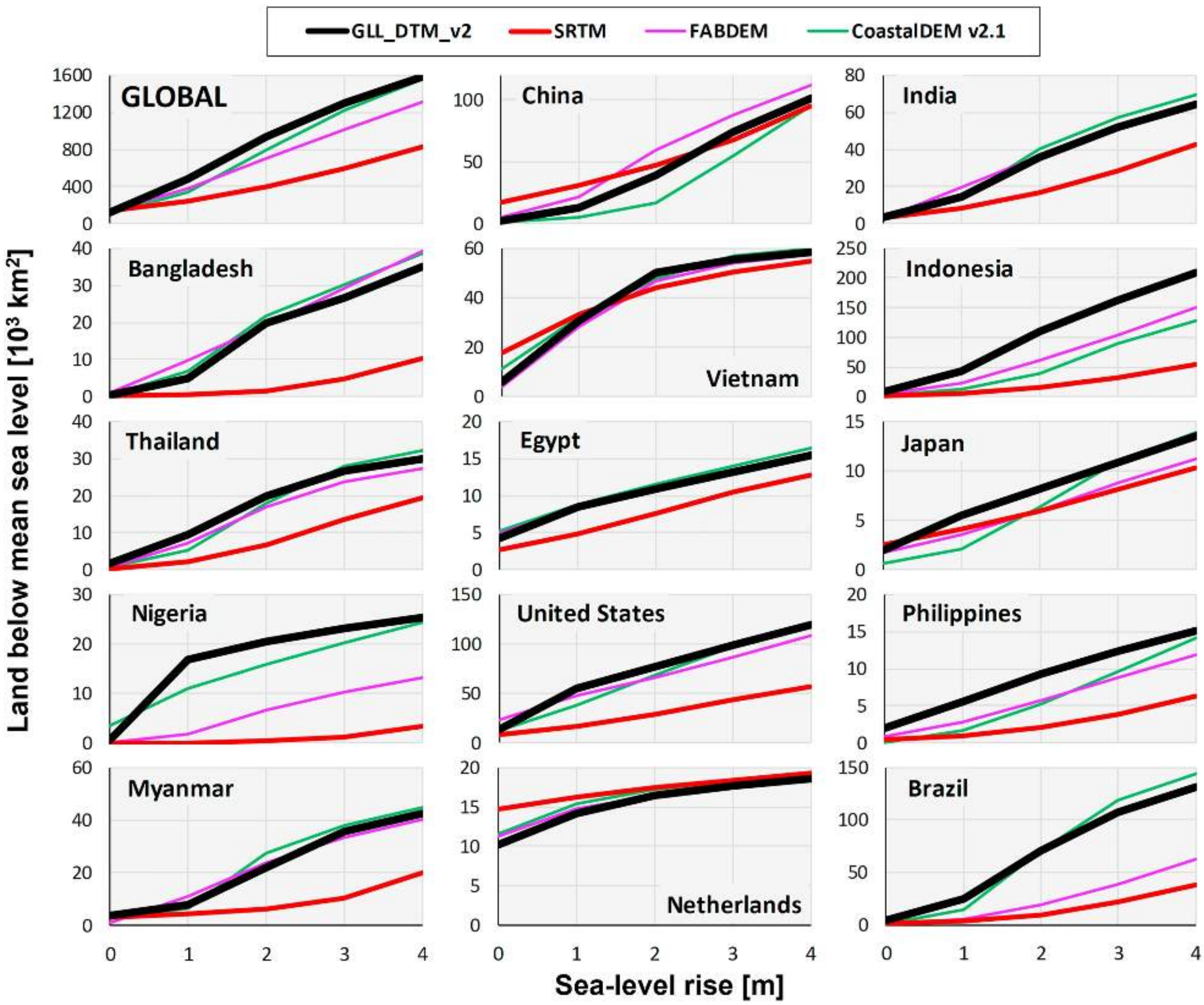

Figure 3. Land area below MSL as SLR progresses. Shown are selected countries with highest lowland population (Table S5 in Supporting Information S1), for the ICESat-2 LiDAR-based GLL_DTM_v2, the most commonly used SRTM and the most recently published CoastalDEM v2.1 and FABDEM that we find to be the most accurate GDEMs after GLL_DTM_v2 (Table 1).

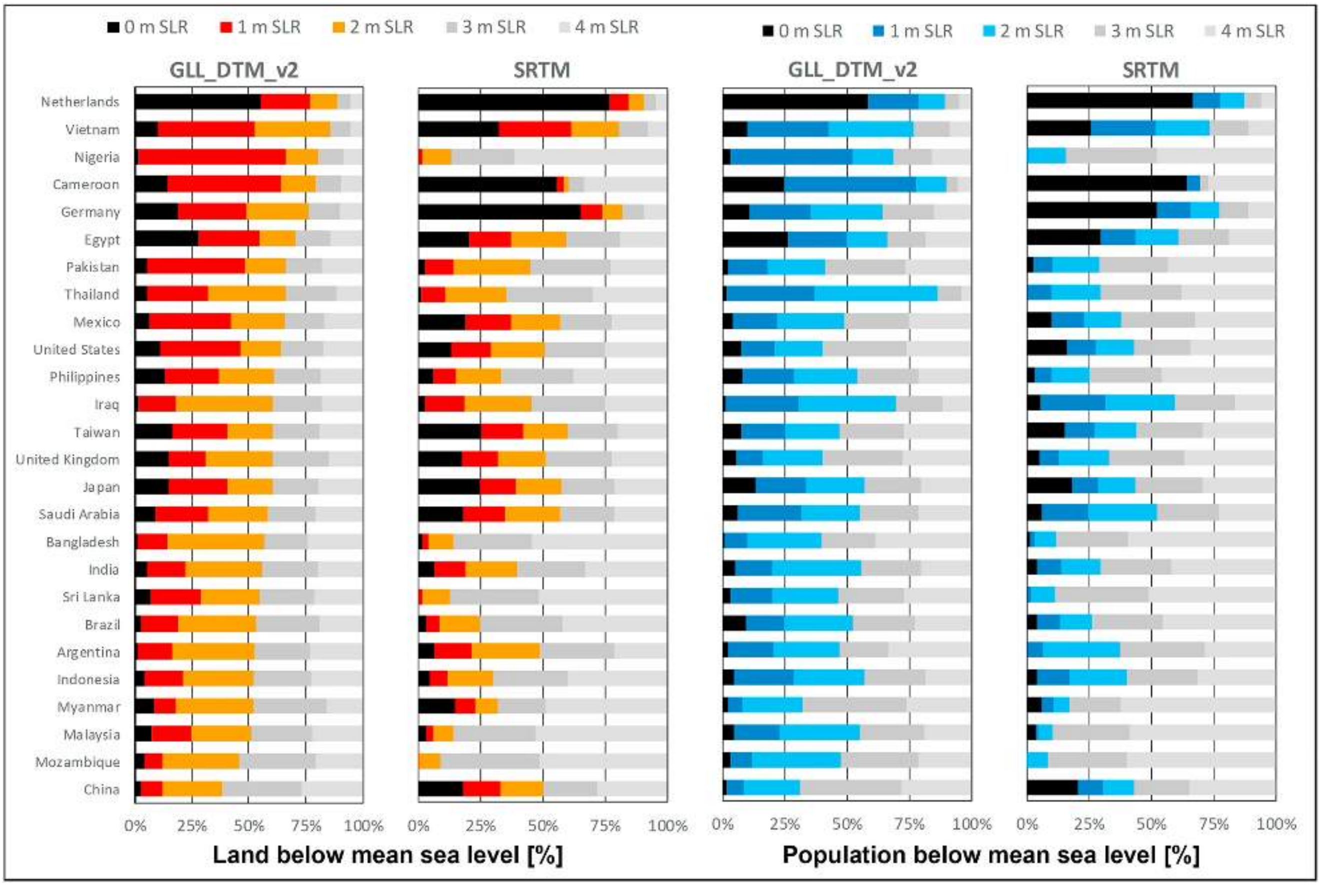

Figure 4. Land and population below mean sea level after different increments of sea-level rise (SLR). Countries shown have at least 2.0 million people currently (2020) living on land that is below 4 m above MSL (GLL_DTM_v2; Table S5 in Supporting Information S1), for GLL_DTM_v2 and SRTM (Table S6 in Supporting Information S1). Countries are ranked by percentage of land below MSL at 2 m SLR according to GLL_DTM_v2. The "0 m SLR" scenario presents the 2020 situation as determined by both elevation datasets.

differences exist here too, most notably in countries with relatively extensive areas of lowland forest (including mangrove) such as Brazil, Nigeria, Philippines and Indonesia, but in the case of CoastalDEM v2.1 also in China and Japan (Figure 3, Figure S5 in Supporting Information S1). Apart from forested areas, we also find differences in urban areas as illustrated for Bangkok where CoastalDEM v2.1 is higher compared to both GLL_DTM_v2 and FABDEM (Figure 1, Figures S5–S6 in Supporting Information S1). Overall, GLL_DTM_v2 is lower than CoastalDEM v2.1 and FABDEM, for 51.0% and 58.3% of the coverage area, respectively. While CoastalDEM v2.1 and FABDEM are generally somewhat higher than GLL_DTM_v2, there are also areas where they are lower (Figure S6 in Supporting Information S1).

The examples of SRTM and other (partly) radar-based GDEMs yielding the greatest underestimation of area below MSL after SLR are mostly of developing countries that rely largely on publicly available global data for risk assessments. Governments of such countries could wrongly conclude that SLR is not of immediate concern to them if they use these GDEMs for flood risk projections. It is worth noting that these GDEMs also sometimes yield unrealistically high areas to be currently below MSL, for instance in The Netherlands and Vietnam (Figures 3 and 4), that are not supported by local more accurate DTMs (Table 1), however this is less likely to negatively affect flood risk assessments as these countries tend to use the local DTMs.

Patterns in population below MSL largely reflect patterns in area below MSL, but are enhanced in some countries. Thailand for example, will see 66% of the land area and as much as 87% of population that is currently below 4 m + MSL becoming below MSL at 2 m SLR, including most of the greater Bangkok area. The corresponding figures for China show the opposite difference with 38% of land and as little as 31% of population (Figure 4, Table S5 in Supporting Information S1).

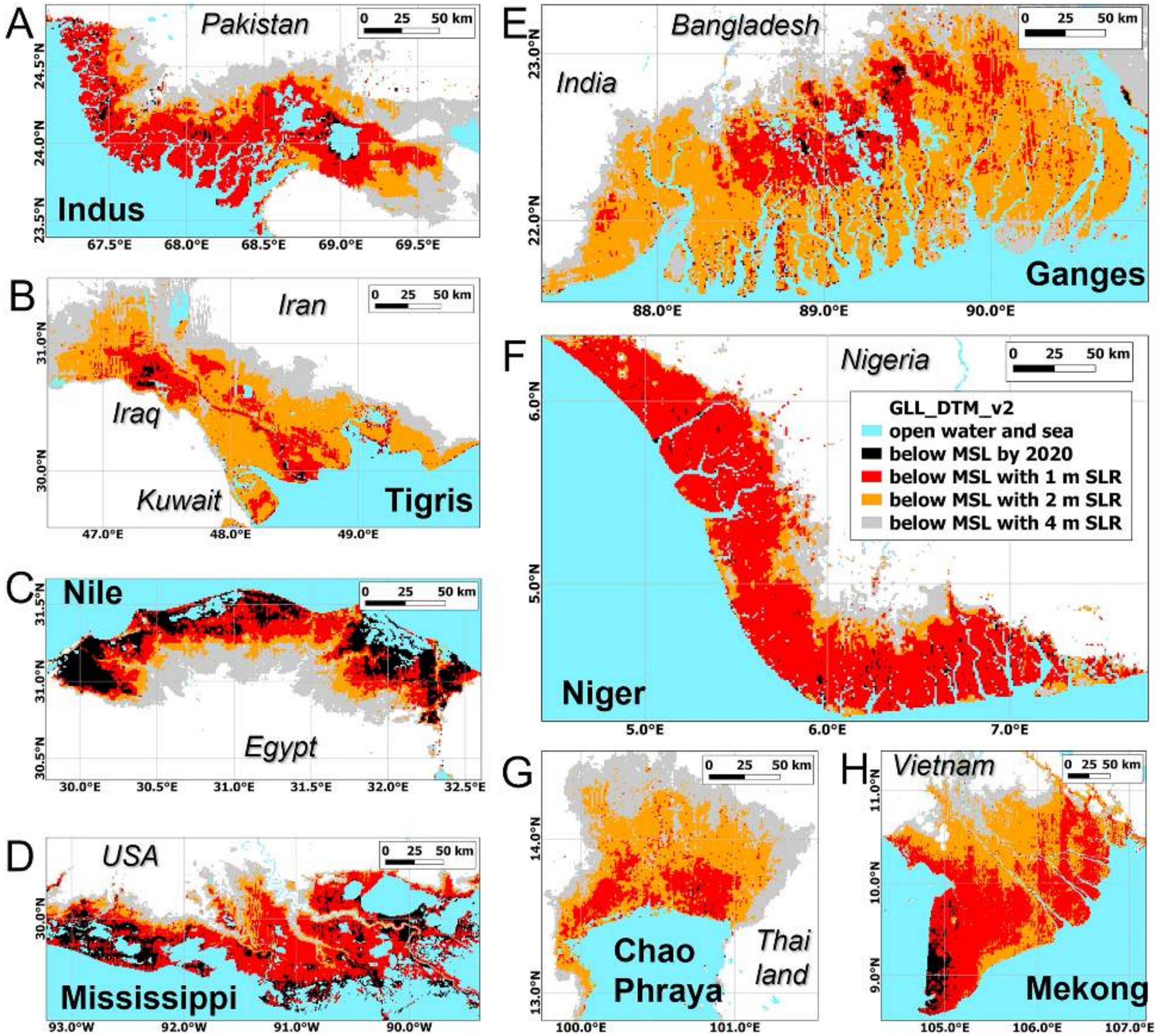

Figure 5. Examples of eight deltas that could potentially be largely flooded with 1 m of SLR, and almost entirely at 2 m SLR. Indicated is the area below mean sea level (MSL) currently (SLR = 0 m) and with 1, 2, or 4 m of SLR. (a) Indus, (b) Tigris, (c) Nile, (d) Mississippi, (e) Ganges, (f) Niger, (g) Chao Phraya, and (h) Mekong.

3.5. Preparation Time for SLR May Be Less Than Expected in Many Countries

The effect on SLR impact projections of using GLL_DTM_v2 instead of earlier GDEMs can be illustrated by comparing the results for 33 deltas highlighted by Syvitski et al. (2009) for having large areas below 2 m + MSL considered to be at high flood risk. Applying GLL_DTM_v2 the overall area below 2 m + MSL across these deltas is 219,621 km^2 whereas it is 91,660 km^2, or 2.4 times less, according to SRTM (Figure 5; Table S1 in Supporting Information S11). In some individual deltas, such as Niger, Irrawaddy and Chao Phraya, the area below MSL yielded by GLL_DTM_v2 is over 5 times the SRTM result. This implies that for these deltas the urgency of flood exposure by SLR and land subsidence is also considerably greater than could be known before satellite LiDAR data became available, demonstrating the importance of using accurate LiDAR-based DEMs when preparing for SLR.

4. Conclusions

The implication of the coastal elevation patterns revealed using a satellite LiDAR-based GDEM is that the world as a whole will see considerably more coastal land below sea level sooner than was indicated by earlier radar-based GDEMs, and consequently will have less time to prepare for the impacts. However, the large regional differences revealed by the same data, suggest that countries will see very different timeline patterns in exposure to flooding. Countries or regions where land will be below MSL sooner than expected, may be encouraged to start preparing for SLR faster. This also highlights the need for high-accuracy local DEMs to plan better. Detailed adaptation and mitigation planning should not rely solely on coarser resolution global elevation data.

This study confirms that assessing areas most vulnerable to SLR will require application of elevation models that are much more accurate than those available until recently (Gesch, 2018; Hooijer & Vernimmen, 2021). Such data are now becoming available globally from satellites carrying LiDAR instruments. Further refinement to horizontal resolutions higher than the ∼1 km offered by GLL_DTM_v2 are possible by merging sparse satellite LiDAR information with the Copernicus DEM radar data that are found to be least inaccurate amongst uncorrected radar-based GDEMs (Table 1), as was done by FABDEM (Hawker et al., 2022). However, while the CoastalDEM v2.1 and FABDEM products demonstrate that combining radar and satellite LiDAR data does achieve improved vertical accuracy compared to earlier products, overall vertical error remains almost twice as high as in GLL_DTM_v2. Particularly in extensive areas of lowland forest and other dense vegetation, and in some urban areas, terrain elevation presented by these products often remains too high (Figure 1, Figures S5 and S6 in Supporting Information S1). In coastal lowlands, that are usually very flat with limited vertical elevation variation over short distances, a lower resolution can therefore result in improved vertical accuracy. For some applications, certainly at the global and regional scale, we propose that achieving optimum vertical accuracy may have higher priority than aspiring to the highest possible horizontal resolution at the cost of vertical accuracy. Although we have demonstrated the overall higher accuracy of GLL_DTM_v2, also compared to higher resolution products, the lower resolution of the product means that there will be limitations in using it for coastal lowlands that are less than a kilometer wide, as well as for some urban areas that have man-made smaller-scale surface topography. The greatest advantage of using GLL_DTM_v2 will therefore be achieved in large deltaic plains and in densely vegetated areas.

The GLL_DTM_v2 elevation data set at ∼1 km horizontal resolution will suffice for such applications and is available in the public domain. It is created in a transparent and replicable way that allows others to build on this work and further refine the model in future as more satellite LiDAR data become available.

Conflict of Interest

The authors declare no conflicts of interest relevant to this study.

Data Availability Statement

The data used in this study are available on Zenodo under https://doi.org/10.5281/zenodo.6534526.

Acknowledgments
The authors want to acknowledge the NASA for providing ICESat-2 LiDAR data, the various Python package developers which allowed efficient data processing and analysis, and QGIS developers for map creation. The authors would like to thank the three anonymous reviewers for their constructive and useful comments and suggestions that enabled us to improve the content of this paper. No external funding was received for this study.

References

Abrams, M., Crippen, R., & Fujisada, H. (2020). ASTER global digital elevation model (GDEM) and ASTER global water body dataset (ASTWBD). *Remote Sensing*, *12*(7), 1156. https://doi.org/10.3390/rs12071156

AHN3. (2019). Retrieved from https://www.ahn.nl

AHN3. (2022). Elevation accuracy (in Dutch). Retrieved from https://www.ahn.nl/kwaliteitsbeschrijving

Airbus. (2020). Copernicus DEM product handbook. Retrieved from https://spacedata.copernicus.eu/documents/20126/0/GEO1988-CopernicusDEM-SPE-002_ProductHandbook_I3.0.pdf

Brodzik, M., Billingsley, B., Haran, T., Raup, B., & Savoie, M. (2014). Correction: Brodzik, M.J., et al. EASE-Grid 2.0: Incremental but Significant Improvements for Earth-Gridded Data Sets. *ISPRS International Journal of Geo-Information* 2012, *1*, 32–45. *ISPRS International Journal of Geo-Information*, *3*(3), 1154–1156. https://doi.org/10.3390/ijgi3031154

Brown, S., Jenkins, K., Goodwin, P., Lincke, D., Vafeidis, A. T., Tol, R. S. J., et al. (2021). Global costs of protecting against sea-level rise at 1.5 to 4.0°C. *Climatic Change*, *167*(1–2), 4. https://doi.org/10.1007/s10584-021-03130-z

Brown, S., Nicholls, R. J., Lázár, A. N., Hornby, D. D., Hill, C., Hazra, S., et al. (2018). What are the implications of sea-level rise for a 1.5, 2 and 3°C rise in global mean temperatures in the Ganges-Brahmaputra-Meghna and other vulnerable deltas? *Regional Environmental Change*, *18*(6), 1829–1842. https://doi.org/10.1007/s10113-018-1311-0

Bunting, P., Rosenqvist, A., Lucas, R., Rebelo, L.-M., Hilarides, L., Thomas, N., et al. (2018). The global mangrove watch—A new 2010 global baseline of mangrove extent. *Remote Sensing*, *10*(10), 1669. https://doi.org/10.3390/rs10101669

Centre for International Earth Science Information Network (CIESIN) - Columbia University. (2018). Gridded population of the world, version 4 (GPWv4): Population density adjusted to Match 2015 revision UN WPP Country totals, revision 11. Palisades NY: NASA socioeconomic data and applications center (SEDAC). https://doi.org/10.7927/H4F47M65

Crippen, R., Buckley, S., Agram, P., Belz, E., Gurrola, E., Hensley, S., et al. (2016). NASADEM Global elevation model: Methods and progress. *The International Archives of the Photogrammetry, Remote Sensing and Spatial Information Sciences*, *XLI-B4*, 125–128. https://doi.org/10.5194/isprs-archives-XLI-B4-125-2016

ESA. (2020). European space agency climate change initiative land cover (ESA CCI LC). In *Annual land cover maps (1992–2020) 300 m*. Retrieved from https://maps.elie.ucl.ac.be/CCI/viewer/

FEMA (2022). Flood risk analysis and mapping (rev. 12), FEMA policy #204-078-1. Retrieved from https://www.fema.gov/sites/default/files/documents/fema_flood-risk-analysis-mapping-policy.pdf

Gesch, D. B. (2018). Best practices for elevation-based assessments of sea-level rise and coastal flooding exposure. *Frontiers of Earth Science*, *6*, 230. https://doi.org/10.3389/feart.2018.00230

Haasnoot, M., Winter, G., Brown, S., Dawson, R. J., Ward, P. J., & Eilander, D. (2021). Long-term sea-level rise necessitates a commitment to adaptation: A first order assessment. *Climate Risk Management*, *34*, 100355. https://doi.org/10.1016/j.crm.2021.100355

Hawker, L., Uhe, P., Paulo, L., Sosa, J., Savage, J., Sampson, C., & Neal, J. (2022). A 30 m global map of elevation with forests and buildings removed. *Environmental Research Letters*, *17*(2), 024016. https://doi.org/10.1088/1748-9326/ac4d4f

Herrera-García, G., Ezquerro, P., Tomás, R., Béjar-Pizarro, M., López-Vinielles, J., Rossi, M., et al. (2021). Mapping the global threat of land subsidence. *Science*, *371*(6524), 34–36. https://doi.org/10.1126/science.abb8549

Hooijer, A., & Vernimmen, R. (2021). Global LiDAR land elevation data reveal greatest sea-level rise vulnerability in the tropics. *Nature Communications*, *12*(1), 3592. https://doi.org/10.1038/s41467-021-23810-9

IPCC. (2021). Summary for policymakers. In V. Masson-Delmotte, P. Zhai, A. Pirani, S. L. Connors, & C. Péan, (Eds.), *Climate change 2021: The physical science basis. Contribution of working group I to the sixth assessment Report of the intergovernmental panel on climate change* (pp. 3–32). Cambridge University Press. https://doi.org/10.1017/9781009157896.001

Jarvis, A., Reuter, H., Nelson, A., & Guevara, E. (2008). *Hole-filled SRTM for the globe version 4, available from the CGIAR-CSI SRTM 90m database* [Report]. Retrieved from http://srtm.csi.cgiar.org

Jevrejeva, S., Jackson, L. P., Grinsted, A., Lincke, D., & Marzeion, B. (2018). Flood damage costs under the sea level rise with warming of 1.5°C and 2°C. *Environmental Research Letters*, *13*(7), 074014. https://doi.org/10.1088/1748-9326/aacc76

Kirezci, E., Young, I. R., Ranasinghe, R., Muis, S., Nicholls, R. J., Lincke, D., & Hinkel, J. (2020). Projections of global-scale extreme sea levels and resulting episodic coastal flooding over the 21st Century. *Scientific Reports*, *10*(1), 11629. https://doi.org/10.1038/s41598-020-67736-6

Koks, E. E., Rozenberg, J., Zorn, C., Tariverdi, M., Vousdoukas, M., Fraser, S. A., et al. (2019). A global multi-hazard risk analysis of road and railway infrastructure assets. *Nature Communications*, *10*(1), 2677. https://doi.org/10.1038/s41467-019-10442-3

Kulp, S. A., & Strauss, B. H. (2021). CoastalDEM v2.1: A high-accuracy and high-resolution global coastal elevation model trained on ICESat-2 satellite lidar (climate central scientific Report) (p. 17). Retrieved from https://www.climatecentral.org/uploads/media/CoastalDEM_2.1_Scientific_Report_.pdf

Liu, A., Cheng, X., & Chen, Z. (2021). Performance evaluation of GEDI and ICESat-2 laser altimeter data for terrain and canopy height retrievals. *Remote Sensing of Environment*, *264*, 112571. https://doi.org/10.1016/j.rse.2021.112571

Marconcini, M., Metz-Marconcini, A., Üreyen, S., Palacios-Lopez, D., Hanke, W., Bachofer, F., et al. (2020). Outlining where humans live, the world settlement Footprint 2015. *Scientific Data*, *7*(1), 242. https://doi.org/10.1038/s41597-020-00580-5

Minderhoud, P. S. J., Coumou, L., Erkens, G., Middelkoop, H., & Stouthamer, E. (2019). Mekong delta much lower than previously assumed in sea-level rise impact assessments. *Nature Communications*, *10*(1), 3847. https://doi.org/10.1038/s41467-019-11602-1

Muis, S., Verlaan, M., Nicholls, R. J., Brown, S., Hinkel, J., Lincke, D., et al. (2017). A comparison of two global datasets of extreme sea levels and resulting flood exposure: Comparison of global extreme sea levels. *Earth's Future*, *5*(4), 379–392. https://doi.org/10.1002/2016EF000430

Mulet, S., Rio, M.-H., Etienne, H., Artana, C., Cancet, M., Dibarboure, G., et al. (2021). The new CNES-CLS18 global mean dynamic topography. *Ocean Science*, *17*(3), 789–808. https://doi.org/10.5194/os-17-789-2021

Neuenschwander, A., & Pitts, K. (2019). The ATL08 land and vegetation product for the ICESat-2 Mission. *Remote Sensing of Environment*, *221*, 247–259. https://doi.org/10.1016/j.rse.2018.11.005

Neuenschwander, A. L., Pitts, K. L., Jelley, B. L., Robbins, J., Klotz, B., Popescu, S. C., et al. (2021). *ATLAS/ICESat-2 L3A land and vegetation height, version 5. ATL08 data product*. NASA National Snow and Ice Data Center Distributed Active Archive Center. https://doi.org/10.5067/ATLAS/ATL08.005

Neumann, B., Vafeidis, A. T., Zimmermann, J., & Nicholls, R. J. (2015). Future coastal population growth and exposure to sea-level rise and coastal flooding - a global assessment. *PLoS One*, *10*(3), e0118571. https://doi.org/10.1371/journal.pone.0118571

Nicholls, R. J., Lincke, D., Hinkel, J., Brown, S., Vafeidis, A. T., Meyssignac, B., et al. (2021). A global analysis of subsidence, relative sea-level change and coastal flood exposure. *Nature Climate Change*, *11*(4), 338–342. https://doi.org/10.1038/s41558-021-00993-z

NOAA. (2020). Retrieved from https://coast.noaa.gov/htdata/raster2/elevation/SLR_viewer_DEM_6230/FL/FL_MFL_dems/

Potapov, P., Li, X., Hernandez-Serna, A., Tyukavina, A., Hansen, M. C., Kommareddy, A., et al. (2021). Mapping global forest canopy height through integration of GEDI and Landsat data. *Remote Sensing of Environment*, *253*, 112165. https://doi.org/10.1016/j.rse.2020.112165

Rio, M.-H., Mulet, S., & Picot, N. (2014). Beyond GOCE for the ocean circulation estimate: Synergetic use of altimetry, gravimetry, and in situ data provides new insight into geostrophic and Ekman currents: Ocean circulation beyond GOCE. *Geophysical Research Letters*, *41*(24), 8918–8925. https://doi.org/10.1002/2014GL061773

Rizzoli, P., Martone, M., Gonzalez, C., Wecklich, C., Borla Tridon, D., Bräutigam, B., et al. (2017). Generation and performance assessment of the global TanDEM-X digital elevation model. *ISPRS Journal of Photogrammetry and Remote Sensing*, *132*, 119–139. https://doi.org/10.1016/j.isprsjprs.2017.08.008

Schuerch, M., Spencer, T., Temmerman, S., Kirwan, M. L., Wolff, C., Lincke, D., et al. (2018). Future response of global coastal wetlands to sea-level rise. *Nature*, *561*(7722), 231–234. https://doi.org/10.1038/s41586-018-0476-5

Syvitski, J. P. M., Kettner, A. J., Overeem, I., Hutton, E. W. H., Hannon, M. T., Brakenridge, G. R., et al. (2009). Sinking deltas due to human activities. *Nature Geoscience*, *2*(10), 681–686. https://doi.org/10.1038/ngeo629

Tadono, T., Nagai, H., Ishida, H., Oda, F., Naito, S., Minakawa, K., & Iwamoto, H. (2016). Generation of the 30 m-mesh global digital surface model by ALOS PRISM. *ISPRS - International Archives of the Photogrammetry, Remote Sensing and Spatial Information Sciences*, *XLI-B4*, 157–162. https://doi.org/10.5194/isprsarchives-XLI-B4-157-2016

Tessler, Z. D., Vorosmarty, C. J., Grossberg, M., Gladkova, I., Aizenman, H., Syvitski, J. P. M., & Foufoula-Georgiou, E. (2015). Profiling risk and sustainability in coastal deltas of the world. *Science*, *349*(6248), 638–643. https://doi.org/10.1126/science.aab3574

10.1029/2022EF002880

Vernimmen, R., Hooijer, A., & Pronk, M. (2020). New ICESat-2 satellite LiDAR data allow first global lowland DTM suitable for accurate coastal flood risk assessment. *Remote Sensing*, *12*(17), 2827. https://doi.org/10.3390/rs12172827

Yamazaki, D., Ikeshima, D., Tawatari, R., Yamaguchi, T., O'Loughlin, F., Neal, J. C., et al. (2017). A high-accuracy map of global terrain elevations: Accurate Global Terrain Elevation map. *Geophysical Research Letters*, *44*(11), 5844–5853. https://doi.org/10.1002/2017GL072874

Zhang, K., Gann, D., Ross, M., Robertson, Q., Sarmiento, J., Santana, S., et al. (2019). Accuracy assessment of ASTER, SRTM, ALOS, and TDX DEMs for Hispaniola and implications for mapping vulnerability to coastal flooding. *Remote Sensing of Environment*, *225*, 290–306. https://doi.org/10.1016/j.rse.2019.02.028

References From the Supporting Information

Hofmann, H., Wickham, H., & Kafadar, K. (2017). Letter-value plots: Boxplots for large data. *Journal of Computational & Graphical Statistics*, *26*(3), 469–477. https://doi.org/10.1080/10618600.2017.1305277

Erratum

In the originally published article, the columns in Table 1 were incorrectly formatted. In the Data Availability Statement, the link to the Zenodo site was incorrectly listed as https://doi.org/10.5281/zenodo.7228643. The columns in Table 1 have been correctly formatted, and the link in the Data Availability Statement has been corrected to https://doi.org/10.5281/zenodo.6534526. This may be considered the authoritative version of record.